Journal of Power Sources 452 (2020) 227760

Contents lists available at ScienceDirect

Journal of Power Sources

journal homepage: www.elsevier.com/locate/jpowsour

Controlling dendrite growth in lithium metal batteries through forced advection

Mihir N. Parekh [a,*], Christopher D. Rahn [a], Lynden A. Archer [b]

[a] Department of Mechanical Engineering, The Pennsylvania State University, University Park, PA, 16802, USA
[b] School of Chemical and Biomolecular Engineering, Cornell University, Ithaca, NY, 14853, USA

HIGHLIGHTS

- Electrolyte flow through porous lithium metal electrode can promote stable plating.
- Increasing the normal flow rate reduces the dendrite growth rate.
- Dendrites are suppressed if Peclet number is greater than critical Peclet number.

GRAPHICAL ABSTRACT

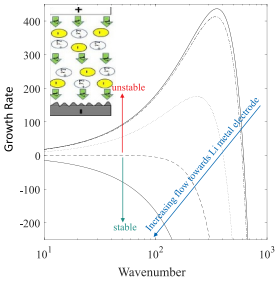

ARTICLE INFO

Keywords:
Lithium metal battery
Dendrite
Advective flow
Stability
Perturbation

ABSTRACT

Instabilities during metal electrodeposition create dendrites on the plating surfaces. In high energy density lithium metal batteries (LMBs) dendrite growth causes safety issues and accelerated aging. In this paper, analytical models predict that dendrite growth can be controlled and potentially eliminated by small advective flows normal to the surface of lithium metal electrode. Electrolyte flow towards the Li metal electrode lowers the dendrite growth rate, overpotential, and impedance. Flow in the opposite direction, however, enhances the dendrite growth. For every current density, there exists a critical velocity above which dendrite growth can be totally eliminated. The critical velocity increases almost linearly with increasing current density. For typical current densities and inter-electrode separation, the critical velocity is very small, indicating the potential for practical application.

1. Introduction

Lithium metal is amongst the highest performing electrodes with remarkable volumetric and gravimetric energy densities [1]. Metallic electrodes suffer from dendrite growth during plating of the lithium cations on the metal surface during charging. As a result, the developed SEI (Solid Electrolyte Interphase) can crack, producing dead Li that contributes to low coulombic efficiency and short cycle life. The cracking of SEI at the dendrite tips in-turn promotes further dendrite growth [2]. Dendrite growth can also lead to internal shorting with potential fires and explosions.

Modelling plays a key role in understanding dendrite growth during electrodeposition. Chazelviel [3] pioneered early work on the effect of mass transport limitations on dendrite growth. Ion depletion is shown to result from converging electric field lines and higher concentration gradients at the dendrite tips. Nishikawa et al. [4], experimentally

* Corresponding author.
E-mail address: mzp523@psu.edu (M.N. Parekh).

https://doi.org/10.1016/j.jpowsour.2020.227760
Received 29 October 2019; Received in revised form 24 December 2019; Accepted 15 January 2020
Available online 7 February 2020

confirm the importance of mass transfer effects in dendrite growth. Considering the role of kinetics, Ely et al. [5] suggest that the dendrite growth rate depends on the applied overpotential with a critical overpotential needed to enable dendrite growth. Akolkar [6] predicts the ratio of dendrite growth rate to the electrodeposition rate by calculating the current at the dendrite tip. Akolkar [7] extends his previous model to include Arrhenius temperature dependence in diffusivity. Yan et al. [8] study the variation in dendrite morphology with temperature gradients perpendicular to the charging direction. However none of these models predict the stability of the electrodeposition process. Sundstrom et al. [9] analyzed electrodeposition stability in binary stagnant electrolytes. Tikekar et al. [10] solved for dendrite growth rate on a perturbed electrode, in case of electrolytes with non-participant anions. Dendrite growth rate increases with increasing wavenumber of the sinusoidal electrode perturbations until it reaches a maximum and then decreases. There is a critical wavenumber above which the perturbation growth rate is negative indicating that dendrites dissolve instead of growing due to the effect of surface tension at the highly curved dendrite tips. In their metallurgical study of electrodeposition, Gireaud et al. [11] identify internal pressure as one of the important factors governing dendrite growth. Modifying the charge-discharge cycle [12–14] by introducing pulses of reverse polarity or rest periods during battery charging to help dissolve dendrites has also been investigated.

Materials-based approaches to dendrite suppression include efforts to stabilize the SEI. Dead Li formed by an unstable SEI, leads to a decrease in coulombic efficiency and capacity [15]. Electrolyte additives [16–19] and protective layers [20,21] on the lithium metal electrode have been shown to stabilize the SEI. Kim et al. [22] and Cheng et al. [23] reduce the effect of high concentration gradients at dendrite tips by developing new materials to make the metal ion flux uniform. Fan et al. [24] observe uniform lithium deposition in their 3D porous structured anode with a large number of polar groups. Li et al. [25] report dendrite free lithium metal anodes by homogenizing and normalizing lithium nucleation and growth on polymer brushes using lithiophilic functional groups. Various innovative techniques have been used to homogenize, localize, or achieve a gradient distribution of lithium ion flux at the lithium metal electrode [26]. Zhang et al. [27] report high areal and volumetric capacity and good cycling performance by reducing dendrite growth using 3D mixed ion electron conductor (MIEC) scaffolds.

Mass transport can also reduce dendrite growth. Yang et al. [28] observe that magnetic stirring of the electrolyte can suppress dendrites. Wang et al. [29] report that the Lorentz force (*jxB*, where *B* is the magnetic field) can eliminate dendrite growth in some situations. From the definition of vector cross product, this force is directed primarily normal to the primary ion flux in a battery cell and as such requires large magnetic fields and/or high interfacial curvature. Tan et al. [30] compute the effects of electro-convection and vortex formation near dendrite tips on dendrite growth and morphology, observing that vortices replenish the electrolyte near the dendrite tips and can alter the dendrite morphology from straight to mossy. Models predict that convection parallel to dendrite surface can also reduce dendrite growth. Crowther et al. [31] did not observe dendrite initiation in their parallel flow experiments. Wlasenko et al. [32] conduct microfluidic experiments with flow normal to the electrode surface and observe limited dendrite growth. Li et al. [33] amplify ionic transport via electrokinetic pumping through a sponge like structure that eliminates dendrite growth.

Following the lead of Tan et al. [30], Li et al. [33] and Wlasenko et al. [32], this paper investigates the effect of advective transport normal to the deposition surface on dendrite growth. Using a first order stability analysis technique, similar to the one used by Tikekar et al. [10], this paper also calculates the dendrite growth rate as a function of normal flow rate and current density.

2. Governing equations

Fig. 1 shows a schematic diagram of the Li metal cell with electrolyte flow. A charging current density $\tilde{\mathbf{J}}(\mathbf{X},\mathbf{T})$ transports Li^+ ions from the positive electrode at $Z=0$ to the Li metal electrode at $Z=L$ where they plate and change the thickness of the anode over time T. The electrodes are assumed to be porous with an imposed electrolyte flow of velocity v along the Z axis. The Li metal electrode could either be perforated or porous (*e.g.* metal foam) to allow normal flow. We assume that the pore structure is sufficiently fine scaled to allow uniform flow.

Within the electrolyte (neglecting the double layer region)

$$\nabla\cdot\tilde{\mathbf{J}}=0. \tag{1}$$

The cation and anion transport equations [10] are given by,

$$\frac{\tilde{\mathbf{J}}}{F}=-D_c\nabla\widetilde{C_c}-\mu_c F\widetilde{C_c}\nabla\tilde{\Phi}+\widetilde{C_c}\mathbf{v} \tag{2}$$

and

$$0=-D_a\nabla\widetilde{C_a}+\mu_a F\widetilde{C_a}\nabla\tilde{\Phi}+\widetilde{C_a}\mathbf{v} \tag{3}$$

where F is Faraday's constant, D is diffusivity, μ is electric mobility, $\tilde{C}(X,Z,T)$ is concentration, $\mathbf{v}=v\hat{\mathbf{k}}$, and $\tilde{\Phi}(X,Z,T)$ is overpotential. The subscripts c and a indicate cation and anion respectively. Electroneutrality requires

$$\widetilde{C_c}=\widetilde{C_a}. \tag{4}$$

The growth rate of the Li metal electrode per unit surface area due to electrodeposition is given by

$$\frac{\partial\widetilde{H_c}}{\partial T}=\left(\frac{v_m}{F}\tilde{\mathbf{J}}\cdot\tilde{\mathbf{n}}\right)\Big|_{\widetilde{H_c}}, \tag{5}$$

where $\widetilde{H_c}$ is the distance between lithium metal electrode and the positive electrode, v_m is the molar volume of Li, and $(\,)|_{\widetilde{H_c}}$ means evaluated at the growing surface $\widetilde{H_c}$. Introducing the non dimensional variables, $\tilde{\mathbf{j}}=\frac{\tilde{\mathbf{J}}L}{FD_cC_0}$, $Pe=\frac{vL}{D_c}$, $\tilde{\varphi}=\frac{\tilde{\Phi}F}{RT}$, $\tilde{c_c}=\frac{\widetilde{C_c}}{C_0}$, $\tilde{c_a}=\frac{\widetilde{C_a}}{C_0}$, $z=\frac{Z}{L}$, $x=\frac{X}{L}$, $M=\left(\frac{D_c}{D_a}+1\right)Pe$, $\tilde{h_c}=\widetilde{H_c}/L$, $k=KL$, and $t=\frac{v_mD_cC_0T}{L^2}$ in Eqs. (1)–(5) produces

$$\nabla\cdot\tilde{\mathbf{j}}=0, \tag{6}$$

$$\tilde{\mathbf{j}}=-\nabla\tilde{c_c}-\tilde{c_c}\nabla\tilde{\varphi}+\tilde{c_c}Pe\hat{\mathbf{k}}, \tag{7}$$

$$0=-\nabla\tilde{c_a}+\tilde{c_a}\nabla\tilde{\varphi}+\tilde{c_a}(M-Pe)\hat{\mathbf{k}}, \tag{8}$$

$$\tilde{c_c}=\tilde{c_a}, \tag{9}$$

$$\frac{\partial\tilde{h_c}}{\partial t}=\tilde{\mathbf{j}}\cdot\tilde{\mathbf{n}}\big|_{\tilde{h_c}}, \tag{10}$$

where C_0 is the average concentration and $\hat{\mathbf{k}}$ is the unit vector in z direction.

The electrochemical energy of the cation at the Li metal boundary is

$$\Psi_c(X,\widetilde{H_c},T)=\Psi_c^0+RT_0ln(\widetilde{C_c}(X,\widetilde{H_c},T))+F\tilde{\Phi}(X,\widetilde{H_c},T) \tag{11}$$

where Ψ_c^0 is the standard electrochemical energy for the electrolyte, R is the universal gas constant, T_0 is the operating cell temperature, and the electrochemical energy in the Li metal electrode is

$$\Psi_m(X,T)=\Psi_m^0+\gamma v_mK(X,T)+F\tilde{\Phi}_m(X,T), \tag{12}$$

where γ is the surface tension at the electrode-electrolyte interface, Ψ_m^0 is the standard electrochemical energy for the electrode, K is the curvature, and $\Phi_m(X,T)$ is the overpotential at the Li metal electrode surface.

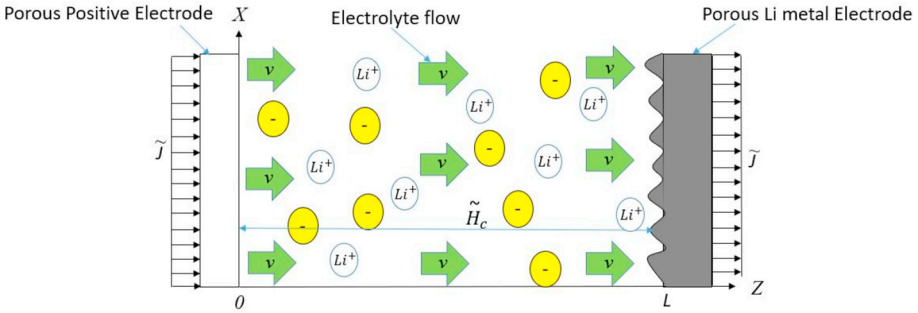

Fig. 1. Schematic diagram of the lithium metal cell model.

At equilibrium, $\Psi_c = \Psi_m$, so

$$\tilde{\Phi}_m = \frac{\Psi_c^0 - \Psi_m^0}{F} + \frac{RT_0}{F}\ln(\widetilde{C_c}(X,\widetilde{H_c},T)) - \frac{\gamma\nu_m K(X,T)}{F} + \tilde{\Phi}(X,\tilde{H}_c,T) \quad (13)$$

The applied charging current density leads to an overpotential of E_0 at the counter-electrode.

$$\tilde{E}_0 = \tilde{\Phi}(X,0,T). \quad (14)$$

Non-dimensionalization of Eqs. (13) and (14) leads us to

$$\tilde{\varphi}_m = \psi_c^0 - \psi_m^0 + \ln(\widetilde{c_c}(x,\widetilde{h_c},t)) - \beta k(x,t) + \tilde{\varphi}(x,\tilde{h}_c,t), \quad (15)$$

$$\tilde{e}_0 = \frac{\tilde{E}_0 F}{RT_0}, \quad (16)$$

$$\tilde{\varphi}(x,0,t) = \tilde{e}_0, \quad (17)$$

where $k = KL$, $\tilde{\varphi}_m = F\tilde{\Phi}_m/(RT_0)$, $\psi_c^0 = \Psi_c^0/(RT_0)$, $\beta = \gamma\nu_m/(RT_0L)$, and $\psi_m^0 = \Psi_m^0/(RT_0)$. Thus, the nondimensional model has only five nondimensional parameters: Pe, j, M, k, β.

3. Base case solutions

For the base case, uniform plating is assumed, so $\tilde{\mathbf{j}}(x,t) = j\hat{\mathbf{k}}$, $\widetilde{c_c}(x,z,t) = c_c(z)$, $\widetilde{c_a}(x,z,t) = c_a(z)$, $\tilde{\varphi}(x,z,t) = \varphi(z)$, $\tilde{e}_0(x,z,t) = e_0$, and $\widetilde{h_c}(x,t) = h_c(t)$. Substitution into Eqs. (7)–(10) along with $K = 0$ for the planar electrode in base case and using the boundary conditions $c_a(0) = c_{a0}$, $\varphi(1) = 0$, and the initial condition $h_c = 1$, and Eq. (17) gives the base case solutions

$$c_c = \frac{j}{M} + \left[c_{a0} - \frac{j}{M}\right]\exp(zM/2), \quad (18)$$

$$\varphi = e_0 + \ln\left[\frac{\left(c_{a0} - \frac{j}{M}\right)\exp\left(\frac{(2Pe-M)z}{2}\right) + \frac{j}{M}\exp((-M+Pe)z)}{c_{a0}}\right], \quad (19)$$

$$c_{a0} = \frac{j}{M} + \frac{\left[1 - \frac{j}{M}\right][M/2]}{\exp(M/2) - 1}, \quad (20)$$

$$h_c = 1 - jt. \quad (21)$$

Critical Peclet number is defined as the Peclet number at which advective flux equals the total ionic flux at the negative electrode, or

$$j = c_c(1)Pe_{cr}. \quad (22)$$

Fig. 2a, b, and 2c show the concentration, overpotential, and electric field profiles for a given current density and various electrolyte velocities using the parameters listed in Table 1. The baseline solution without flow ($Pe = 0$) shows the concentration decreasing, from the positive electrode to the lithium metal electrode. The overpotential decreases from $\varphi(0) = 1$ to the boundary condition, $\varphi(1) = 0$. The electric field increases with a maximum at the negative electrode. These results agree with previous research [10]. Increasing the velocity reduces the concentration, overpotential gradients, and the electric field from the baseline case of $Pe = 0$. At $Pe = Pe_{cr}$, the ion concentration is almost uniform at $c_c = 1$, $\varphi = 0$, and $d\varphi/dz = 0$. Increase of Pe above Pe_{cr} reverses the concentration and overpotential gradients. Fig. 3b shows that higher flow rates lower the overpotential at the

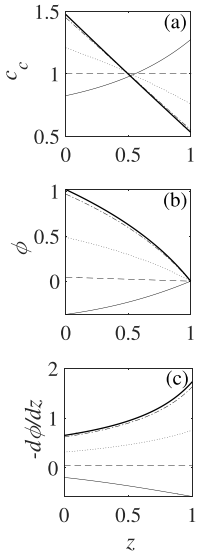

Fig. 2. Base case solutions of non-dimensionalized (a) Concentration, (b) Overpotential and (c) Electric field at $j = 1.8$: $Pe = 1.5Pe_{cr}$ (solid), $Pe = Pe_{cr}$ (dashed), $Pe = 0.5Pe_{cr}$ (dotted), $Pe = 0$ (dashed-dotted), and $Pe = -0.05Pe_{cr}$ (bold).

Table 1
Parameters used in the model.

Property	Value
C_0	1 M
T_0	300 K
L	1 mm
D_a	$4E-10\ m^2s^{-1}$ [10]
D_c	$10^{-11}\ m^2s^{-1}$ [7]
F	96500 $Cmol^{-1}$
R	$8.314 Jmol^{-1}K^{-1}$
γ	$1.716\ Nm^{-1}$ [10]
μ_c	$D_c/(RT_0)mols^{-1}N^{-1}$
μ_a	$D_a/(RT_0)mols^{-1}N^{-1}$
ν_m	$1.33E-5\ molm^{-3}$ [10]

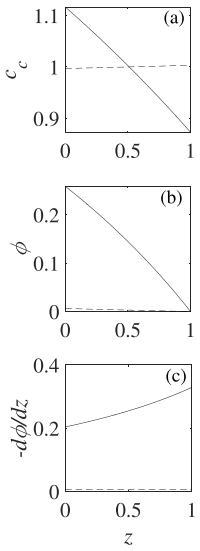

Fig. 3. Base case solutions of non-dimensionalized (a) Concentration, (b) Overpotential, and (c) Electric field at $Pe = 0.5$, $M = 0.51$ for $j = 0.5$ (dashed) and $j = 1$ (solid).

counter-electrode surface. This phenomenon stems from the fact that some of the energy required to move the Li^+ ions from the counter-electrode to the Li metal electrode is supplied by the fluid flow, thus reducing the required electrical power.

Fig. 3a, b, and 3c show the concentration, overpotential, and electric field at a given flow rate ($Pe = 0.5$) and various charging current densities. Higher current leads to higher concentration and overpotential gradients at the Li metal electrode surface. Thus, diffusion and migration fluxes are higher at higher current densities and potentially can lead to higher dendrite growth rates [3,10].

Fig. 4 shows the critical Peclet number versus j. For small j, the concentration is approximately uniform, so $c_c(1) = 1$ and $j = Pe_{cr}$. The critical Peclet number is on the order of 1, so the dimensional critical velocity is on the order of D_c/L. For $j = 1.8$ and parameters in Table 1, the critical velocity is roughly 1.75 $nm\ s^{-1}$ which means that the fluid particles would take approximately a week to cross the inter-electrode gap by advective flux. Thus, the required flow rate is very low and may be practically achieved using a variety of low power methods. As shown in Fig. 4, the critical Peclet number is independent of temperature. It depends only on current density. The critical velocity, however, reduces with reducing temperature because the diffusivity reduces with reducing temperature [7].

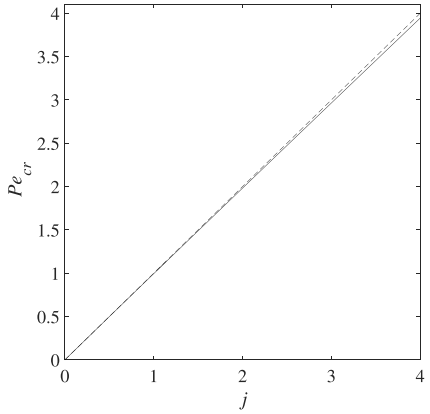

Fig. 4. Critical Peclet number versus non-dimensional current density (solid) and a linear approximation (dashed).

4. Stability analysis

To analyze the stability of electroplating on the Li metal surface, we introduce the first order sinusoidal perturbation,

$$\widetilde{h_c} = h_c + h_c' exp(\sigma t) exp(ikx), \tag{23}$$

where k, h_c' and σ are the nondimensional wavenumber, nondimensional amplitude, and non dimensional exponential growth rate. The wavenumber equals $2\pi/\lambda$ where λ is the wavelength. Dendrites are assumed to grow exponentially fast for σ greater than 0 and decay for σ less than 0. To eliminate dendrites, the electrode must be stable ($\sigma < 0$) for dendrites of all sizes (k). The perturbation growth rate (σ) is a function of wavenumber (k) as dendrites with different curvatures may grow with different rates due to the effect of surface tension, varying concentration of electric field line, and varying concentration gradient on the curved dendrite tip. The positive electrode surface at $z = 0$ has not been perturbed because no dendrites grow from the positive electrode during charging.

The concentration, overpotential, and current density are assumed to have the same spatial and temporal dependencies:

$$\widetilde{c_c} = c_c + c_c' exp(\sigma t) exp(ikx), \tag{24}$$

$$\tilde{\varphi} = \varphi + \varphi' exp(\sigma t) exp(ikx), \tag{25}$$

$$\tilde{\mathbf{j}} = j\widehat{\mathbf{k}} + \mathbf{j}' exp(\sigma t) exp(ikx), \tag{26}$$

where c_c', φ', and j' are the non-dimensional amplitudes of the perturbations in cation concentration, overpotential, and current density respectively. We assume that the porous electrodes are sufficiently thick and that the electrolyte storage tank is sufficiently far enough. Using Darcy's law in the porous electrode, creeping flow in the gap between two electrodes, continuity of pressure and velocity perturbations across the porous electrode-electrolyte interface, and zero pressure and velocity perturbations at the outlet of porous electrode and in the electrolyte storage tank drives velocity perturbations throughout the domain to zero. Hence, in this paper velocity perturbations have been assumed to be zero for simplicity. However, this may not always be the case and hence the authors intend to do a detailed analysis which involves velocity perturbations in the future.

Substitution of Eqs. (24)–(26) into Eqs. 7- 9 yields

$$\varphi' = \frac{c_c'}{c_c} \tag{27}$$

Eq. (26) and Eq. (10) imply

$$\sigma h_c' = 2\frac{dc_c'}{dz}(1) - Mc_c' \tag{28}$$

Eqs. (11) and (12) give

$$\frac{c_c'(1)}{c_c(1)} + \frac{1}{c_c(1)}\frac{dc_c}{dz}(1)h_c' + \varphi'(1) + \frac{d\varphi}{dz}(1)h_c' = -\beta h_c' k^2 \tag{29}$$

Solving the above equations leads to the following solution for the perturbation growth rate σ

$$\sigma = \frac{c_c(1)}{2}\left[\frac{-1}{c_c(1)}\frac{dc_c}{dz}(1) - \frac{d\varphi}{dz}(1) - \beta k^2\right]\left[2\frac{m_1 exp(m_1) - m_2 exp(m_2)}{exp(m_1) - exp(m_2)} - M\right], \tag{30}$$

where $m_1 = \frac{M+\sqrt{M^2+16k^2}}{4}$ and $m_2 = \frac{M-\sqrt{M^2+16k^2}}{4}$.

Critical wavenumber,

$$k_{cr} = \sqrt{\frac{1}{\beta}\left[\frac{-1}{c_c(1)}\frac{dc_c}{dz}(1) - \frac{d\varphi}{dz}(1)\right]}, \tag{31}$$

is the wavenumber above which $\sigma < 0$.

Fig. 5 shows the non-dimensional dendrite growth rate at a given current density and various flow rates versus non-dimensional wavenumber.

For a given charging current and a flow rate, σ increases with k and then decreases. This is because with increasing curvature, the concentration of electric field lines and the concentration gradient at the dendrite tip increase, leading to higher dendrite growth. However, as can be seen from Eq. (12), higher k also increases the required surface energy per mole of electrodeposited Li and thus acts as a deterrent to the increase of σ with k. In agreement with Tikekar et al. [10], the zero flow case has an unstable Li metal electrode ($\sigma > 0$) for $k < 597$. Flow towards the Li metal electrode during charging reduces the dendrite growth rate. In fact, above the critical flow rate, σ ¡0 for all wavenumbers. In other words, supercritical flow can entirely stabilize the Li metal electrode. Subcritical flow rates may not completely stabilize the electrode but the peak height and range of unstable wavenumbers ($k < k_{cr}$) are both reduced, thus reducing the level of electrode instability. If the critical wavenumber is sufficiently small, then the size of the unstable growth will be large and not dendritic, potentially exceeding the physical size of the electrode and eliminating dendrite growth as a practical concern. Flow in the wrong direction, however, can enhance the dendrite growth rate.

This model does not explicitly account for breakage and reformation of SEI. SEI breakage occurs due to multiple reasons, including the large volume change associated with plating and stripping Li from under the SEI and excessive tensile stress at the dendrite tips. Large volume changes can lead to inhomogeneities in the SEI layer that may initiate dendrites. At the dendrite tips, SEI may fail under excessive tensile stress [2]. The stress itself depends on curvature. For sinusoidal perturbations with infinitesimally small amplitude studied in this work, the dendrite tip curvature is proportional to the amplitude and the square of the wavenumber. For low wavenumbers, the curvature is infinitesimally small and the tensile stress on the SEI at the dendrite tips is infinitesimally small, so, the SEI will not break. In regions where the electrode is stable, the small initial perturbations decay with time.

Table 2 explains the stabilizing effect of normal flow. Diffusion, migration and advection flux add together to produce the total Li^+ ion flux at different flow velocities. Increasing the flow rate increases the contribution of advection relative to migration and diffusion. Thus, increasing flow rate in the direction of total flux helps reduce dendrite growth rate and critical wavenumber. This result is in agreement with the explanation for dendrite growth rate given by Aryanfar et al. [14]. At the critical velocity ($Pe = Pe_{cr}$), total flux equals the advective flux at the lithium metal electrode, so diffusion and migration fluxes sum to zero. As shown by dashed line for critical velocity in Fig. 5, this totally eliminates dendrite growth. However, in Table 2, the small value of $\sigma = 1.15$ at $Pe = Pe_{cr}$ is because of numerical error. In fact, if advective flux is more than total flux the dendrites dissolve instead of growing.

Fig. 6 shows the non-dimensional perturbation growth rate versus k for a given flow rate at various current densities. Higher current leads to higher growth rate at the same wavenumber. This result is as per the expectations because at zero current, the dendrite growth rate should be zero.

5. Conclusion

This paper shows that electrolyte flow towards the Li metal electrode lowers the dendrite growth rate, reduces the required overpotential, and reduces the impedance. Flow in the opposite direction, however, enhances the dendrite growth. For every current density, there exists a critical velocity above which dendrite growth can be totally eliminated. As shown in Fig. 4, the critical velocity increases almost linearly with increasing current density. For typical current densities and inter-electrode separation, the critical velocity is very small, indicating the potential for practical application. Supercritical flow is very small and could be achieved by several possible mechanisms, including microfluidic pumping systems [34] along with porous or micropatterned electrodes [35–37]. It may also be achieved by programmed squeezing deformations of a battery pack composed of pouch cells.

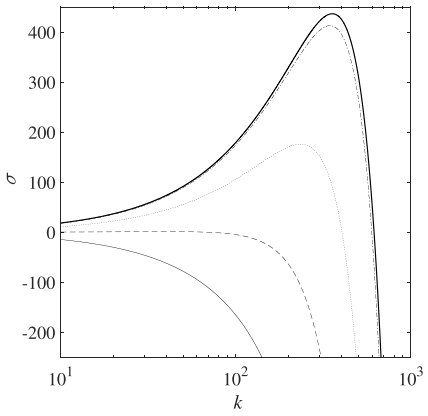

Fig. 5. Non-dimensional growth rate vs non-dimensional wavenumber at $j = 1.8$, $Pe = 1.5Pe_{cr}$ (solid), $Pe = Pe_{cr}$ (dashed), $Pe = 0.5Pe_{cr}$ (dotted), $Pe = 0$ (dashed dotted), and $Pe = -0.05Pe_{cr}$ (bold).

Table 2
Normalized Li^+ ion flux contributions at $z = 1$ and maximum non-dimensionalized perturbation growth rate versus flow rate for $j = 1.8$

Pe/Pe_{cr}	Diffusion	Migration	Advection	σ_{max}	k_{cr}
−0.05	0.514	0.513	−0.0264	437	615
0	0.5	0.5	0	413	597
0.5	0.307	0.316	0.378	176	403
1.	−0.0125	0.0125	1	1.15	69
1.5	−0.482	−0.434	1.91	−0.734	0

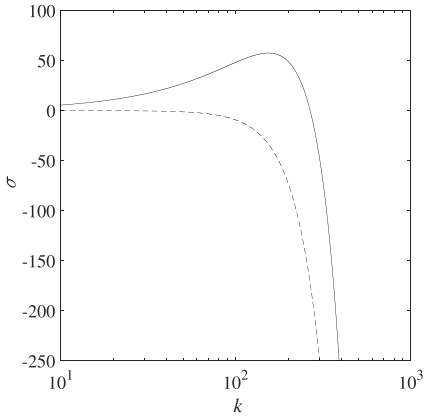

Fig. 6. Non-dimensional growth rate vs non-dimensional wavenumber at $Pe = 0.5$, $M = 0.51$, $j = 2j_{cr}$ (solid) and $j = j_{cr}$ (dashed). Here j_{cr} is defined as the value of j for which $Pe = 0.5 = Pe_{cr}$.

Declaration of competing interest

The authors declare that they have no known competing financial interests or personal relationships that could have appeared to influence the work reported in this paper.

Acknowledgement

This research was partially supported by the National Science Foundation under Grant No. 1662055. We would like to thank Dr.

Donald L. Koch of School of Chemical and Biomolecular Engineering, Cornell University for our fruitful discussions.

References

[1] M.S. Whittingham, Proc. IEEE 100 (2012) 1518–1534.
[2] G. Liu, W. Lu, J. Electrochem. Soc. 164 (2017) A1826–A1833.
[3] J.-N. Chazalviel, Phys. Rev. 42 (1990) 7355.
[4] K. Nishikawa, T. Mori, T. Nishida, Y. Fukunaka, M. Rosso, J. Electroanal. Chem. 661 (2011) 84–89.
[5] D.R. Ely, R.E. García, J. Electrochem. Soc. 160 (2013) A662–A668.
[6] R. Akolkar, J. Power Sources 232 (2013) 23–28.
[7] R. Akolkar, J. Power Sources 246 (2014) 84–89.
[8] H. Yan, Y. Bie, X. Cui, G. Xiong, L. Chen, Energy Convers. Manag. 161 (2018) 193–204.
[9] L.-G. Sundström, F.H. Bark, Electrochim. Acta 40 (1995) 599–614.
[10] M.D. Tikekar, L.A. Archer, D.L. Koch, J. Electrochem. Soc. 161 (2014) A847–A855.
[11] L. Gireaud, S. Grugeon, S. Laruelle, B. Yrieix, J.-M. Tarascon, Electrochem. Commun. 8 (2006) 1639–1649.
[12] H. Yang, E.O. Fey, B.D. Trimm, N. Dimitrov, M.S. Whittingham, J. Power Sources 272 (2014) 900–908.
[13] M.Z. Mayers, J.W. Kaminski, T.F. Miller III, J. Phys. Chem. C 116 (2012) 26214–26221.
[14] A. Aryanfar, D. Brooks, B.V. Merinov, W.A. Goddard III, A.J. Colussi, M. R. Hoffmann, J. Phys. Chem. Lett. 5 (2014) 1721–1726.
[15] K.-H. Chen, K.N. Wood, E. Kazyak, W.S. LePage, A.L. Davis, A.J. Sanchez, N. P. Dasgupta, J. Mater. Chem. 5 (2017) 11671–11681.
[16] G. Li, Y. Gao, X. He, Q. Huang, S. Chen, S.H. Kim, D. Wang, Nat. Commun. 8 (2017) 850.
[17] J. Zheng, M.H. Engelhard, D. Mei, S. Jiao, B.J. Polzin, J.-G. Zhang, W. Xu, Nature Energy 2 (2017) 17012.
[18] J. Qian, W.A. Henderson, W. Xu, P. Bhattacharya, M. Engelhard, O. Borodin, J.-G. Zhang, Nat. Commun. 6 (2015) 6362.
[19] L. Suo, Y.-S. Hu, H. Li, M. Armand, L. Chen, Nat. Commun. 4 (2013) 1481.
[20] Y. Liu, D. Lin, P.Y. Yuen, K. Liu, J. Xie, R.H. Dauskardt, Y. Cui, Adv. Mater. 29 (2017) 1605531.
[21] B. Zhu, Y. Jin, X. Hu, Q. Zheng, S. Zhang, Q. Wang, J. Zhu, Adv. Mater. 29 (2017) 1603755.
[22] P.J. Kim, K. Kim, V.G. Pol, Electrochim. Acta 283 (2018) 517–527.
[23] X.-B. Cheng, T.-Z. Hou, R. Zhang, H.-J. Peng, C.-Z. Zhao, J.-Q. Huang, Q. Zhang, Adv. Mater. 28 (2016) 2888–2895.
[24] L. Fan, H.L. Zhuang, W. Zhang, Y. Fu, Z. Liao, Y. Lu, Advanced Energy Materials 8 (2018) 1703360.
[25] N. Li, Q. Ye, K. Zhang, H. Yan, C. Shen, B. Wei, K. Xie, Angew. Chem. Int. Ed. 58 (50) (2019) 18246–18251.
[26] C. Wang, A. Wang, L. Ren, X. Guan, D. Wang, A. Dong, C. Zhang, G. Li, J. Luo, Adv. Funct. Mater. 29 (49) (2019), 1905940.
[27] C. Zhang, S. Liu, G. Li, C. Zhang, X. Liu, J. Luo, Adv. Mater. 30 (2018) 1801328.
[28] X. Yang, Z. Wen, X. Zhu, S. Huang, Solid State Ionics 176 (2005) 1051–1055.
[29] A. Wang, Q. Deng, L. Deng, X. Guan, J. Luo, Adv. Funct. Mater. (2019) 1902630.
[30] J. Tan, E.M. Ryan, J. Power Sources 323 (2016) 67–77.
[31] O. Crowther, A.C. West, J. Electrochem. Soc. 155 (2008) A806–A811.
[32] A. Wlasenko, F. Soltani, D. Zakopcan, D. Sinton, G. Steeves, Phys. Rev. 81 (2010), 021601.
[33] G. Li, Z. Liu, Q. Huang, Y. Gao, M. Regula, D. Wang, L.-Q. Chen, D. Wang, Nature Energy 3 (2018) 1076.
[34] B.D. Iverson, S.V. Garimella, Microfluid. Nanofluidics 5 (2008) 145–174.
[35] J. Park, J. Jeong, Y. Lee, M. Oh, M.-H. Ryou, Y.M. Lee, Advanced Materials Interfaces 3 (2016) 1600140.
[36] M.-H. Ryou, Y.M. Lee, Y. Lee, M. Winter, P. Bieker, Adv. Funct. Mater. 25 (2015) 834–841.
[37] S.-H. Wang, Y.-X. Yin, T.-T. Zuo, W. Dong, J.-Y. Li, J.-L. Shi, C.-H. Zhang, N.-W. Li, C.-J. Li, Y.-G. Guo, Adv. Mater. 29 (2017) 1703729.